Smart Structures and Systems, *Vol. 26, No. 6 (2020) 721-733*
DOI: https://doi.org/10.12989/sss.2020.26.6.721

Optimal placement of piezoelectric actuator/senor patches pair in sandwich plate by improved genetic algorithm

Amir Amini[1,2a], Mehdi Mohammadimehr[*3] and Alireza Faraji[2b]

[1]*Department of Control, Faculty of Computer and Electrical Engineering, University of Kashan, Kashan, Iran*
[2]*Institute of Material and Energy, Iranian space research center, Isfahan, Iran*
[3]*Department of Solid Mechanics, Faculty of Mechanical Engineering, University of Kashan, Kashan, Iran*

(*Received January 26, 2020, Revised September 26, 2020, Accepted October 18, 2020*)

Abstract. The present study investigates the employing of piezoelectric patches in active control of a sandwich plate. Indeed, the active control and optimal patch distribution on this structure are presented together. A sandwich plate with honeycomb core and composite reinforced by carbon nanotubes in facesheet layers is considered so that the optimum position of actuator/sensor patches pair is guaranteed to suppress the vibration of sandwich structures. The sandwich panel consists of a search space which is a square of 200 × 200 mm with a numerous number of candidates for the optimum position. Also, different dimension of square and rectangular plates to obtain the optimal placement of piezoelectric actuator/senor patches pair is considered. Based on genetic algorithm and LQR, the optimum position of patches and fitness function is determined, respectively. The present study reveals that the efficiency and performance of LQR control is affected by the optimal placement of the actuator/sensor patches pair to a large extent. It is also shown that an intelligent selection of the parent, repeated genes filtering, and 80% crossover and 20% mutation would increase the convergence of the algorithm. It is noted that a fitness function is achieved by collection actuator/sensor patches pair cost functions in the same position (controllability). It is worth mentioning that the study of the optimal location of actuator/sensor patches pair is carried out for different boundary conditions of a sandwich plate such as simply supported and clamped boundary conditions.

Keywords: optimum position of piezoelectric patches; improved genetic algorithm; vibration suppression; composite sandwich plate; LQR control

1. Introduction

Piezoelectric actuators have been of great practical use in suppressing disturbances and shape control of flexible structures. For example, the significant role of piezoelectric actuators in suppressing large amplitude vibrations can be seen in large space structures such as solar arrays (Rudolf *et al*. 2010, Martynowicz 2019). However, with the main role of weight in space structures, most of them have to be ultra-light-weight, which leads to the use of only a limited number of piezoelectric actuators.

The classical methods have been used to obtain the optimum position of patches but these methods are generally non-convex, which is considered as a downside. For instance, Xue *et al*. (2018) suppressed vibration of floor panels by the modal filtering technique. In the another study, Jia and Shan (2018) investigated a novel optimization index in the spillover effects based on the control force and B-spline elements were used for the purpose of discretizing the Partial Differential Equations (PDEs) of flexoelectricity (Ghasemi *et al*. 2018). Their study is slowed in terms of the convergence approach.

Stochastic methods such as Genetic Algorithm (GA) and Particle Swarm Optimization (PSO) in which there is no hypothesis about the cost function or the constraints (Argha *et al*. 2019, Manohar *et al*. 2018, Nestorović *et al*. 2015) can be suggested to solve such problems. Indeed, these methods are used the inlet searching technique to find an approximate solution in optimization problems.

Several problems in modeling and control of stochastically-driven dynamical systems can be considered as regularized semi-definite programs. Zare *et al*. (2018) examined two representative problems and they showed that can be formulated in a similar manner. Using a coupling technique, Yassin *et al*. (2018) investigated an efficient hybrid optimization approach.

In another study, using Regulated Genetic Algorithm (RGA), Sakha *et al*. (2017) proposed the optimum position of patches in large-scale switched systems. By measuring oscillation amplitude, Daraji *et al*. (2017) obtained the best optimum location of patches. Furthermore, using New Modified Cuckoo Search Algorithm (NMCSA), Yang *et al*. (2018) proposed an optimal placement of patches for active control. Babaeeian and Mohammadimehr (2020) investigated the time elapsed effect on residual stress measurement in a composite plate by DIC method. Mohammadimehr *et al*. (2018a) investigated bending,

*Corresponding author, Associate Professor,
E-mail: mmohammadimehr@kashanu.ac.ir
[a] Ph.D. Student, E-mail: a.amini@grad.kashanu.ac.ir; a.amini@isrc.ac.ir
[b] Assistant Professor, E-mail: arfaraji@kashanu.ac.ir

ISSN: 1738-1584 (Print), 1738-1991 (Online)

buckling, and free vibration analyses of carbon nanotube reinforced composite beams and experimental tensile test to obtain the mechanical properties of nanocomposite.

Based on Finite Element Method (FEM) and First-order Shear Deformation Theory (FSDT), the optimal placement and active control of laminated composite plates is developed by Tham *et al*. (2018). Bendine *et al*. (2019) developed LQR method to find the optimum position of patches. A novel relaxation sequential Dijkstra's algorithm was proposed by Yin *et al*. (2019).

The gradient based methods, which are more accurate than stochastic methods, have also been used by researchers. Nanthakumar *et al*. (2017) used a regularized level set method to detect material interfaces of the piezoelectric structure in which an algorithm is proposed to solve the inverse problem of detecting inclusion interfaces and the extended finite element method is used to analyze the structure per iteration. In the same study, Ghasemi *et al*. (2017) employed a design methodology based on a combination of isogeometric analysis to optimize topology of piezoelectric/flexoelectric materials. The fourth order PDEs of flexoelectricity were discretized using non-uniform rational B-spline. With the growing research space, the drawback of gradient based methods would be their time-consuming nature.

Ghorbanpour Arani *et al*. (2016) depicted surface stress and agglomeration effects on nonlocal biaxial buckling polymeric nanocomposite plate reinforced by CNT using various approaches. Mohammadimehr *et al*. (2016) considered the effect of size-dependent effect on biaxial and shear nonlinear buckling analysis of nonlocal isotropic and orthotropic micro-plate based on surface stress and modified couple stress theories. In the other work, Rajabi and Mohammadimehr (2019) illustrated bending analysis of a micro sandwich skew plate using extended Kantorovich method based on Eshelby-Mori-Tanaka approach. AkhavanAlavi *et al*. (2019) presented active control of micro Reddy beam integrated with functionally graded nanocomposite sensor and actuator based on linear quadratic regulator method. Mohammadimehr and Mehrabi (2018) studied electro-thermo-mechanical vibration and stability analyses of double-bonded micro composite sandwich piezoelectric tubes conveying fluid flow. Mohammadimehr *et al*. (2017) depicted the effect of non-local higher order stress to predict the nonlinear vibration behavior of carbon nanotube conveying viscous nanoflow.

In this study, obtaining the optimal placement of piezoelectric actuator/senor patches pair in sandwich plate with honeycomb core and carbon nanotube reinforced composite facesheets by improved genetic algorithm is a lack of the previous study and the novelty of the present study. Based on genetic algorithm, the optimal patch distribution for suppressing vibration in a sandwich plate is investigated. A sandwich plate with Carbon Nanotubes (CNTs) as reinforcement in facesheets and honeycomb core is considered. The equations of motion are illustrated in the state space. Using the classical plate theory, the equations of motion is derived for the sandwich plate. Using LQR, the fitness function is obtained. What makes the study different is the researchers' attempt to add the sensor position to the cost function. The optimum placement of actuator/sensor patches pair is obtained by improved GA with defining fitness function for a sandwich plate. The using intelligent methods decrease complication of analytical solution for big research spaces. When the number of actuator/sensor patches pair increase and the research space becomes infinite, the stochastic methods such as neural network and genetic algorithm will be the best option. The removal of the repeated gene and the proper selection of the parent population decrease convergence time and develop a mutation method which guarantees the global optimization. The different boundary conditions of a sandwich plate such as simply supported and clamped boundary conditions are investigated. Based on the difference of cost function with its previous value, this research may be able to change the number of bit in the mutation. Mutation in the built chromosomes is guaranteed the global optimization.

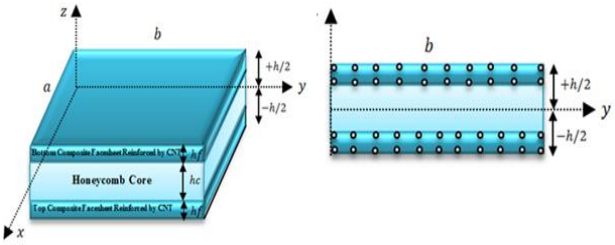

Fig. 1 A schematic view of sandwich plate with CNT symmetric distribution in facesheets and honeycomb core

2. Mathematical model representation

Sandwich plates are made of a homogenous aluminum honeycomb core and two Carbon Nanotubes Reinforced Composite (CNTRC) facesheets with different weight fractions of CNT. The sandwich panel with length a, width b and thickness h is shown in Fig. 1.

The classical displacement fields for the sandwich plate are expressed as (Rostami *et al*. 2019)

$$\begin{cases} U(x,y,z,t) = u(x,y,t) - z\dfrac{\partial w(x,y,t)}{\partial x} \\ V(x,y,z,t) = v(x,y,t) - z\dfrac{\partial w(x,y,t)}{\partial y} \\ W(x,y,z,t) = w(x,y,t) \end{cases} \tag{1}$$

where u, v and w denote the displacements of the middle plate (Appendix A).

Since the displacements are not noticeable, the values of U and V can be ignored. Vibration mode shapes method is applied to simplify the system equations. Using the time and position separation method, we have

$$w(x,y,t) = N^T(x,y)\Gamma(t) \tag{2}$$

where N and Γ contain the shape functions and modal coordinates, respectively.

Table 1 Mode shapes and natural frequencies

S.N		Boundary conditions	Mode shapes
1	*X* direction	Fixed-free	$\mathrm{N}(x)=\sin\left(\frac{m\pi}{2a}x\right)$
	Y direction	Fixed-free	$\mathrm{N}(y)=\sin\left(\frac{n\pi}{2b}y\right)$
2	*X* direction	Simply-simply supported	$\mathrm{N}(x)=\sin\left(\frac{m\pi}{a}x\right)$
	Y direction	Simply-simply supported	$\mathrm{N}(y)=\sin\left(\frac{n\pi}{b}y\right)$
3	*X* direction	Free-free	$\mathrm{N}(x)=\cos\left(\frac{m\pi}{a}x\right)$
	Y direction	Free-free	$\mathrm{N}(y)=\cos\left(\frac{n\pi}{b}y\right)$

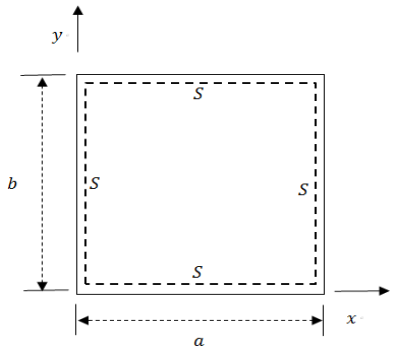

Fig. 2 All simply supported (SSSS) boundary conditions edges for sandwich plate

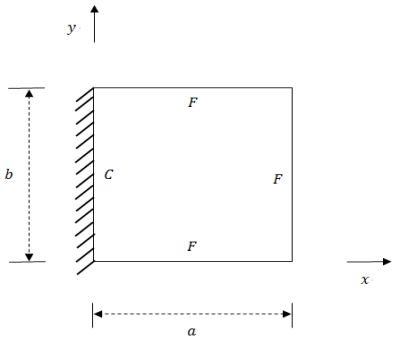

Fig. 3 All Clamped-three free edges (CFFF) boundary condition in sandwich plate

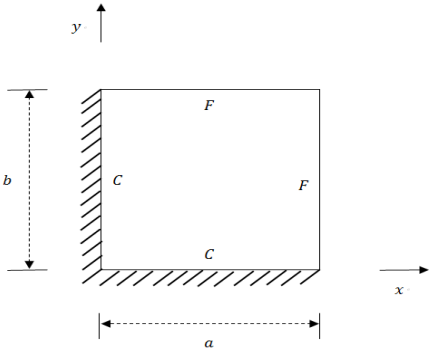

Fig. 4 Two clamped-two free edges (CCFF) boundary condition in sandwich plate

The form of the solutions of N (x, y), i.e., the mode shapes, will depend on the types of boundary conditions. The three most common boundary conditions of sandwich plate in Fig. 1 are shown in Table 1 (Dorato *et al*. 2000). Table 1 presents the equations for various mode shapes with different boundary conditions such as fixed-free, simply-simply supported and free-free boundary conditions.

In general, the mode shapes of the sandwich plate in three different boundary conditions including all simply supported (SSSS) edges, clamped-three free edges (CFFF), two clamped-two free edges (CFFC) are shown in Figs. 2, 3 and 4, respectively (Aglietti *et al*. 2004)

$$N_{m,n}(x,y)=\sin\left(\frac{m\pi x}{a}\right)\sin\left(\frac{n\pi y}{b}\right) \tag{3}$$

$$N_{m,n}(x,y)=\sin\left(\frac{m\pi x}{2a}\right)\cos\left(\frac{n\pi y}{b}\right) \tag{4}$$

$$N_{m,n}(x,y)=\sin\left(\frac{m\pi x}{2a}\right)\sin\left(\frac{n\pi y}{2b}\right) \tag{5}$$

The equations of motion are derived based on Hamilton's principle as follows (Alipour and Zareian 2008, Ghasemi and Meskini 2019)

$$\begin{cases} L=T-U \\ \dfrac{d}{dt}\left(\dfrac{\partial L}{\partial \dot{q}_i}\right)-\dfrac{\partial L}{\partial q_i}=Q_i \end{cases} \tag{6}$$

where T, U, q_i and Q_i are shown in Appendix B.

Q is expressed by point forces that act on the sandwich plate in the coordinate system as follows

$$Q=N_f^T F \tag{7}$$

where F and N_f column vectors are external forces and modal shape, respectively, at the corresponding force locations.

By substituting Eqs. (B17)-(B18) into Eq. (B15), the governing equation can be written as follows

$$\begin{gathered} M\ddot{\Gamma}C_s\dot{\Gamma}+K_{elast}\Gamma+K_{pza_{elastelect}}^T V_{pza}=N_f^T F \\ K_{pz_{elastelect}}\Gamma+K_{pz_{elastelect}}^T V_{pz}=0 \end{gathered} \tag{8}$$

where

$$K_{pz_{elastelect}}^T V_{pz}=\begin{bmatrix}K_{pzs_{elastelect}}^T & K_{pza_{elastelect}}^T\end{bmatrix}\begin{bmatrix}\mathrm{V_{pzs}}\\ \mathrm{V_{pza}}\end{bmatrix}$$

where $[M]$, $[K]$, $[F]$, $[V_{pza}]$ are the global mass matrix, the global stiffness matrix, the external force vector, and the control force vector, respectively. $[C_s]=\alpha[M]+\beta[K]$ is the damping matrix of which α and β are the constants.

The procedure to obtain the governing Eq. (8) has been shown in Appendix B (Amini *et al*. 2019).

To solve the Eq. (8) (or Eq. (B14) in Appendix B) based on LQR that is an analytical method, the cost function is found. Then using genetic algorithm that is a numerical method, the optimal placement of piezoelectric actuator/ senor patches pair in sandwich plate is obtained.

3. Space state representation

The obtained mathematical model from Eq. (8) can be expressed as

$$W_{out} = C_w x \tag{9}$$

$$V_s = C_v x \tag{10}$$

$$\dot{x} = Ax + B_v V_a + B_f F \tag{11}$$

where

$$\begin{cases} x = \begin{pmatrix} x_1 \\ x_2 \end{pmatrix} = \begin{pmatrix} \Gamma \\ \dot{\Gamma} \end{pmatrix}, \begin{cases} \dot{x}_1 = x_2 \\ \dot{x}_2 = -M^{-1}Kx_1 - M^{-1}C_s x_2 \\ -M^{-1}K^T_{pza_{elastelect}} V_{pza} + M^{-1}N_f{}^T F \end{cases} \\ y = C_v x_1 \end{cases} \tag{12}$$

Therefore

$$\mathrm{A} = \begin{bmatrix} 0 & \mathrm{I} \\ -M^{-1}K & -M^{-1}C_s \end{bmatrix}, \quad B_v = \begin{bmatrix} 0 \\ -M^{-1}K^T_{pza_{elastelect}} \end{bmatrix}, \quad B_f = \begin{bmatrix} 0 \\ M^{-1}N_f^T \end{bmatrix} \tag{13}$$

$$C_v = \left[-K_{pzs_{elect}}{}^{-1} K_{pzs_{elastelect}} \; 0\right], \quad C_w = [N^T_{out} \; 0] \tag{14}$$

where K denotes the total stiffness matrix and W_{out} is the output displacement of the sandwich panel specified by N_{out} that is the vibration mode shape vectors.

4. LQR control and objective function

To solve the Eq. (8) based on LQR that is an analytical method, the cost function is found.

4.1 Optimum position of actuator patches

The cost function is considered as (Demetriou and Borggard 2003, Ilchmann *et al*. 2018, Ogata 2010)

$$\mathrm{J}(v_a) = \int_0^\infty \{x^T(t)Qx(t) + V_a^T(t)RV_a(t)\}\,\mathrm{dt} \tag{15}$$

where the symmetric weighting matrices Q and R are positive semi-definite and positive definite, respectively. By adding disturbance to Eq. (15), we have

$$\mathrm{J}(v_a) = \int_0^\infty \{x^T(t)Qx(t) + V_a^T(t)RV_a(t) - \gamma^2|w(t)|^2\}\mathrm{dt} \tag{16}$$

In the present study, the optimal value of the cost function is given by (Demetriou 2000, Rao *et al*. 2014a, b)

$$V_{pza}(t) = -R^{-1}Bv^T(\eta)P_c(\eta)x(t) \tag{17}$$

$$A^T P_c(\eta) + P_c(\eta)A - P_c(\eta)B_v(\eta)R^{-1}B_v^T(\eta)P_c(\eta) + Q = 0 \tag{18}$$

The optimal value of the cost functional is then given by

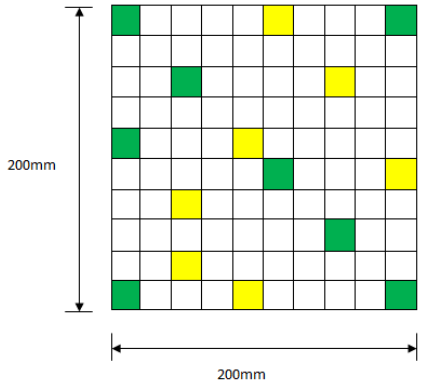

Fig. 5 Some of the possible positions in the search space

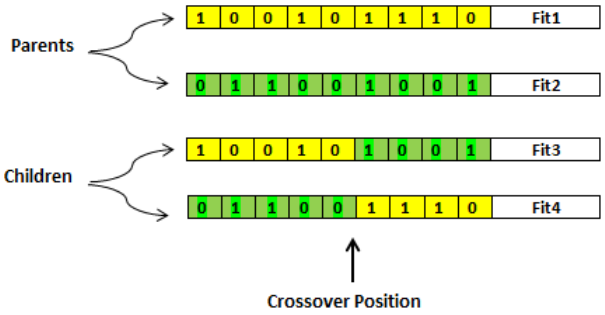

Fig. 6 Crossover gives off-spring of two children with new fitness values

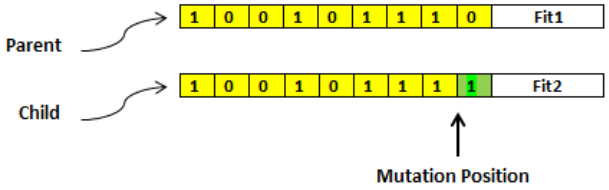

Fig. 7 Mutation gives off-spring of a child with new fitness value

$$J_{opt} = \mathrm{tr}[P(\eta)] \tag{19}$$

4.2 Optimum placement of actuator/sensor patches pair

When the LQR cost is taken to be (Kumar and Narayanan 2007, Ashwin *et al*. 2009)

$$\mathrm{J}(v_a) = \int_0^\infty \{y^T(t)Qy(t) + V_a^T(t)RV_a(t)\}\,\mathrm{dt} \tag{20}$$

The state estimate of $x(t)$ is defined as

$$\dot{\hat{x}}(\mathrm{t}) = A\hat{x}(t) + B_v(\eta)u(t) + L(\eta)(y(t) - C_v(\eta)\hat{x}(t)) \tag{21}$$

$$\hat{y}(t) = C_v(\eta)\hat{x}(t) \tag{22}$$

The observer gain $L(\eta) = H(t)C_v{}^T(\eta)M^{-1}$ can be found, where $H(\eta)$ is obtained by solving the (sensor)

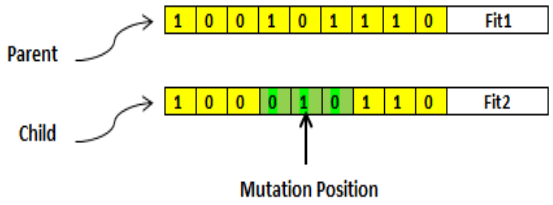

Fig. 8 Mutation with three bit change gives off-spring of a child with improved fitness value

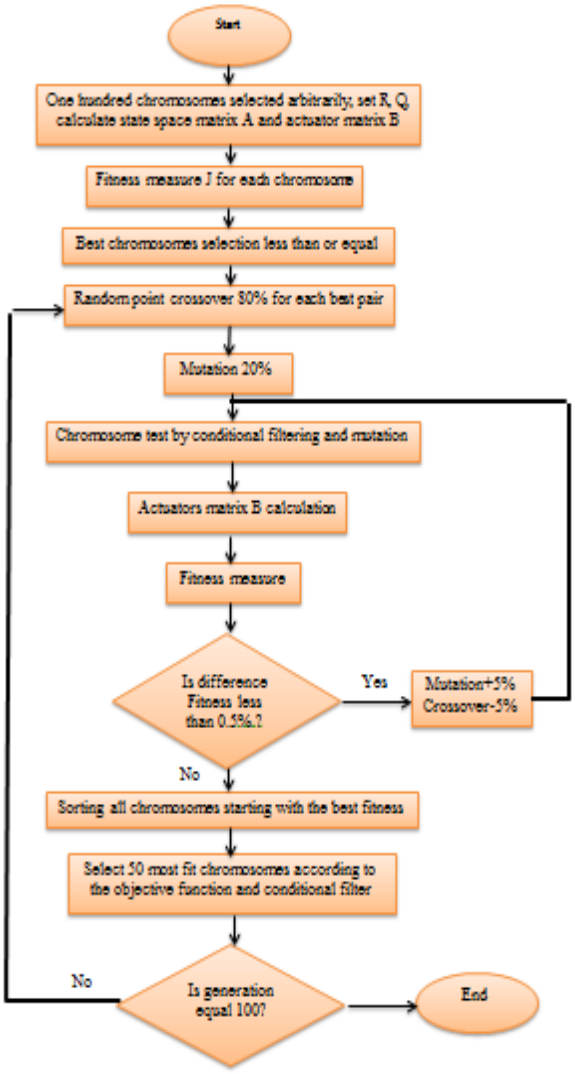

Fig. 9 Block diagram of genetic algorithm placement strategy

location-parameterized filter Riccati equation.

$$AH(\eta) + H(\eta)A^T + \tilde{Q} - H(\eta)C_v^T(\eta)M^{-1}C_v(\eta)H(\eta) = 0 \quad (23)$$

In this case, the optimum position of actuator/sensor patches pair is obtained as follows (Kumar and Narayanan 2007).

$$J_{opt} = \text{tr}\{P(\eta)H(\eta)C_v^T(\eta)R^{-1}C_v(\eta)H(\eta) + H(\eta)Q\}$$
$$H(\eta) + H(\eta)A^T + \tilde{Q} - H(\eta)C_v^T(\eta)M^{-1}C_v(\eta)H(\eta) \quad (24)$$

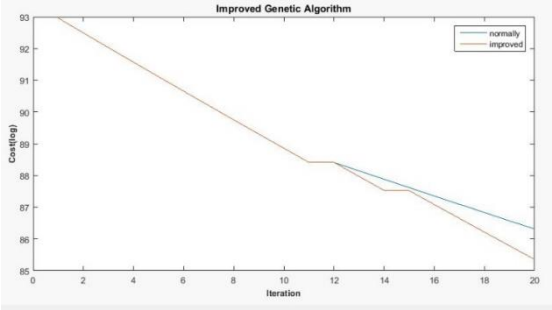

Fig. 10 Comparison of cost values in the normal and improved genetic algorithms

Table 2 The comparison of the cost values in the improved and normal genetic algorithms for 20 iterations

	Genetic algorithm			Improved genetic algorithm		
Iteration	Mutation	Crossover	Cost (logarithmic value)	Mutation	Crossover	Cost (logarithmic value)
1	0.20	0.80	92.9583	0.20	0.80	92.9583
2	0.20	0.80	92.4935	0.20	0.80	92.4935
3	0.20	0.80	92.0310	0.20	0.80	92.0310
4	0.20	0.80	91.5708	0.20	0.80	91.5708
5	0.20	0.80	91.1130	0.20	0.80	91.1130
6	0.20	0.80	90.6574	0.20	0.80	90.6574
7	0.20	0.80	90.2041	0.20	0.80	90.2041
8	0.20	0.80	89.7531	0.20	0.80	89.7531
9	0.20	0.80	89.3043	0.20	0.80	89.3043
10	0.20	0.80	88.8578	0.20	0.80	88.8578
11	0.20	0.80	88.4135	0.20	0.80	88.4135
12	0.20	0.80	88.4113	0.20	0.80	88.4113
13	0.20	0.80	88.1460	0.25	0.75	87.9692
14	0.20	0.80	87.8816	0.25	0.75	87.5294
15	0.20	0.80	87.6179	0.25	0.75	87.5217
16	0.20	0.80	87.3551	0.30	0.70	87.0840
17	0.20	0.80	87.0930	0.30	0.70	86.6486
18	0.20	0.80	86.8317	0.30	0.70	86.2154
19	0.20	0.80	86.5712	0.30	0.70	85.7843
20	0.20	0.80	86.3115	0.30	0.70	85.3554

Thus, Eq. (24) gives the optimum cost function to find the best position for enhanced piezoelectric patches pair.

For non-collocated pair, we have a serious problem, i.e., time (delay). In fact, when a sensor senses a vibration or change in placement, it takes actuator some time (delay) to show a proper reaction and damp this vibration. For this problem, adaptive control can be a good choice for controller.

5. Improved genetic algorithm

Stochastic method i.e., GA is less complicated than the

Table 3 Mechanical properties of materials for sandwich plates

	Material dimensions	Material properties
CNTRC facesheet	$a = 200$ mm $b = 200$ mm $h = 0.5$ mm	$E1 = 5.64$ TPa $E2 = 7.08$ TPa $G12 = 1.94$ TPa $V_{CNT} = 0.17$ $\eta_1 = 0.142, \eta_2 = 1.626, \eta_3 = 1.138$ $\rho = 4000$ kgm^{-3} $\upsilon = 0.175$
Aluminum core 5052	$a = 200$ mm $b = 200$ mm $h = 20$ mm	$E1 = 0.41$ GPa $E2 = 0.24$ GPa $G12 = 0.22$ GPa $\rho = 37$ kgm^{-3} $\upsilon = 0.33$
Piezoelectric patch	$hpzs = 0.19$ mm	$E = 63e9$ Pa $\rho = 7650$ kgm^{-3} $\upsilon = 0.3$ $D = 1.66e - 10$ mv^{-1} $\varepsilon = 1700\ \varepsilon^0$

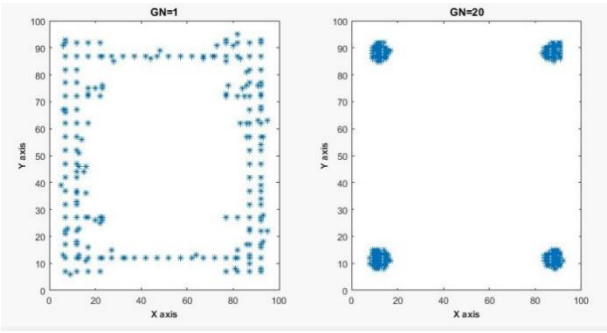

(a)

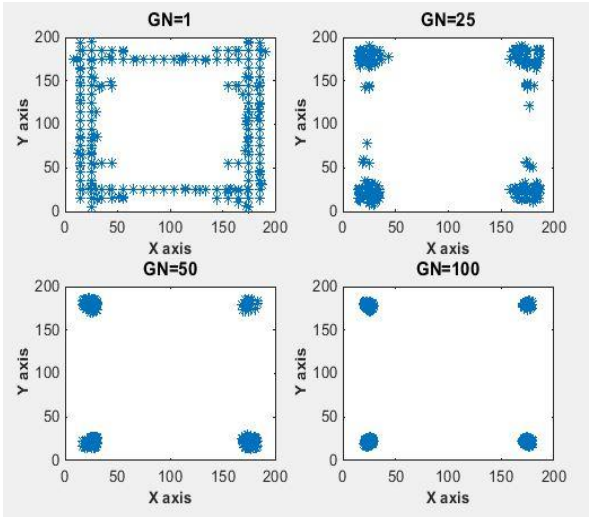

(b)

Fig. 11 The optimal locations of the patches in the SSSS condition in 2-dimentional space for a square plate in dimensions (a) 100 mm × 100 mm; (b) 200 mm × 200 mm

gradient based method when the number of patches increases. With a good training and selection of a proper

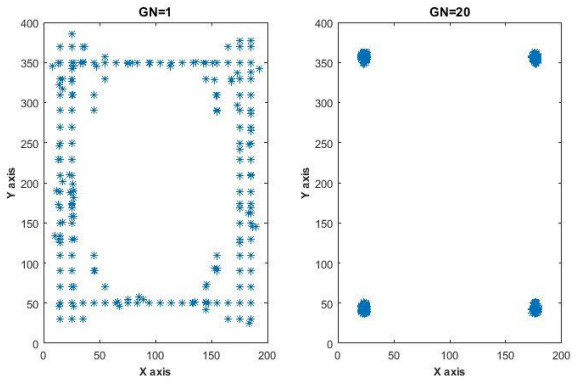

(a)

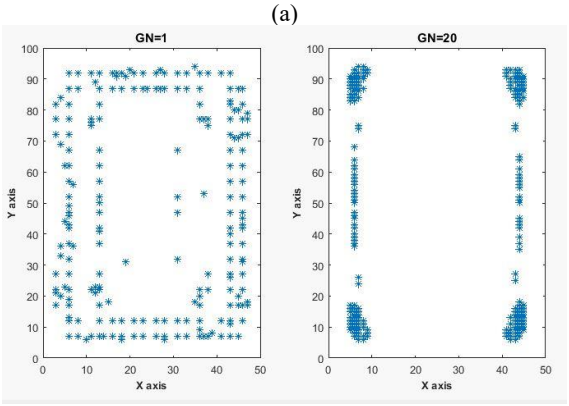

(b)

Fig. 12 The optimal locations of the patches in the SSSS condition in 2-dimentional space for a rectangular plate in dimensions (a) 200 mm × 400 mm; (b) 50 mm × 100 mm

first population, stochastic methods can reach the global optimization sooner.

Some problems for gradient based methods are as follows:

- They don't respond to non-differentiable functions.
- They are complicated methods to solve.
- Their convergence is hard to prove.

Thus, in this research, the improved genetic algorithm is employed. Using this method that is a numerical method, the optimal placement of piezoelectric actuator/senor patches pair in sandwich plate is obtained by defining fitness function for a sandwich plate with the dimensions 200 mm × 200 mm and piezoelectric patches with the dimensions 20 mm × 20 mm. Thus, the search space contains at least 32400 positions for a piezoelectric patch (Fig. 5).

Each population consists of the chromosomes each made of the positions (x) and (y) which are defined as binary digits ($2^8 = 256$) representing the locations of a piezoelectric patch on the plate. For example, the positions $x = 28$ mm and $y = 130$ mm are a chromosome with two binary digits 00011100 and 10000010. Therefore, the genetic algorithm acts twice, once for the position x and once for the position y.

Figs. 6-7 show two chromosomes that are selected from the marked search space as fitness value $Fit1$ and $Fit2$ whose values are obtained from the chromosome gene

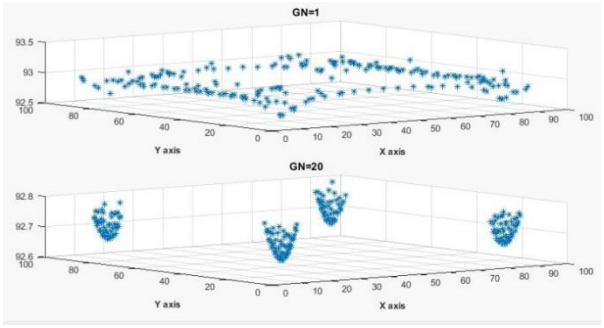

(a)

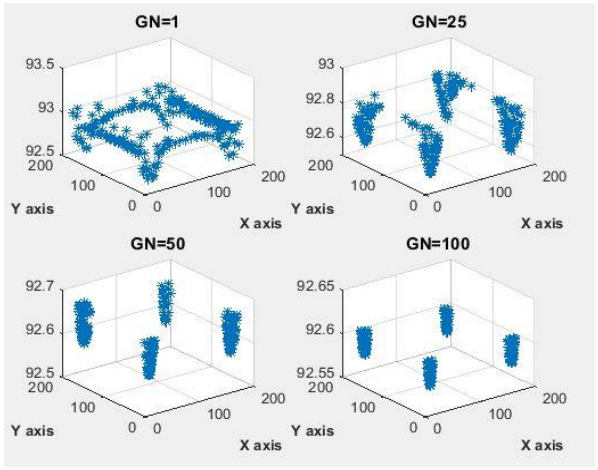

(b)

Fig. 13 The optimal locations of the patches in the SSSS condition in 3-dimentional space for a square plate in dimensions (a) 100 mm × 100 mm; (b) 200 mm × 200 mm

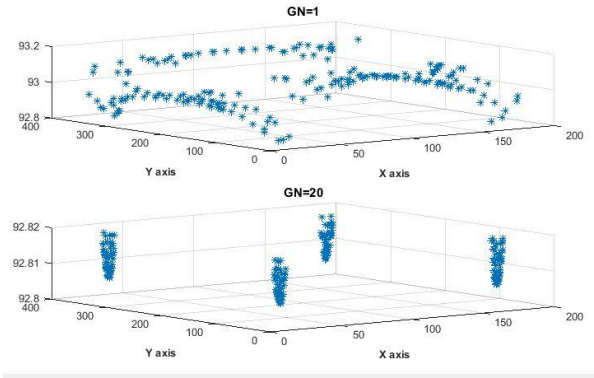

(a)

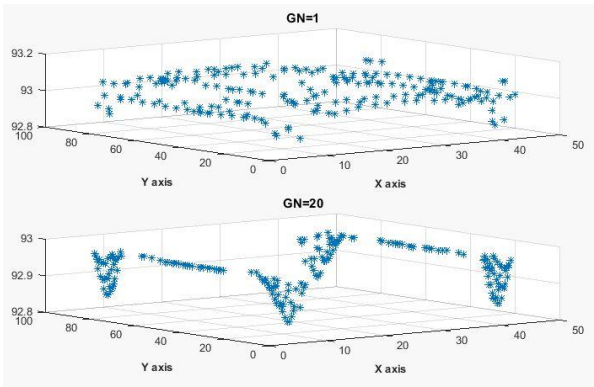

(b)

Fig. 14 The optimal locations of the patches in the SSSS condition in 3-dimentional space for a rectangular plate in dimensions (a) 200 mm × 400 mm; (b) 50 mm × 100 mm

properties. These chromosomes represent the two parents. For the illustrated case, crossover occurs randomly at some point along the chromosomes to produce the two child chromosomes (Fig. 6). In addition, mutation has 20% of child generations (Fig. 7).

Suitable values of $Q(\tilde{Q}) = 10^{11}$ and $R(M) = 1$ are set by the user. The removal of the repeated gene and the proper selection of the parent population decrease convergence time and develop a mutation method which guarantees the global optimization. Given the cost function, the number of bits in the mutation method is changeable.

That is, if the gradient of cost function value decreases, the number of bits in the mutation method increases. That is, after per iteration in GA, if the fitness value decrease of the previous step is not less than 0.5%, the mutation percentage will then increase to 5%. Thus, the number of contribution bits of the chromosome will be increased up to three bits in generation and the convergence occurs faster to obtain the global optimization. In Figs. 8-9, the three-bit change and the increasing percentage of mutation are shown. Block diagrams of genetic algorithm strategy can be seen in Fig. 9.

In Fig. 10 and Table 2, the improved genetic algorithm for SSSS condition is shown. The amount of mutation is changed twice and the cost value decreases more in compared to the normal state.

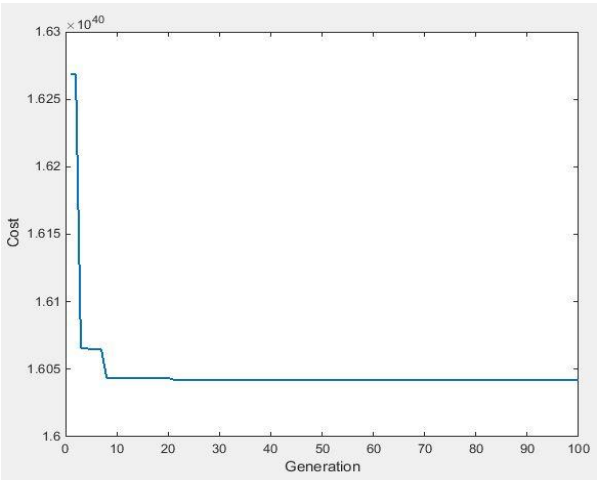

Fig. 15 Variation of fitness value with generation in the SSSS condition

6. Results and discussion

Table 3 shows the mechanical and geometry properties of the sandwich plate and patches (Mohammadimehr *et al*. 2018b and Tanimoto *et al*. 2001). In order to determine the optimum placement of the actuator/sensor patches pair, the GA is used with the following values: ps = 100; pc = 0.8; pm = 0.2; N = 100. The sandwich plate is under different

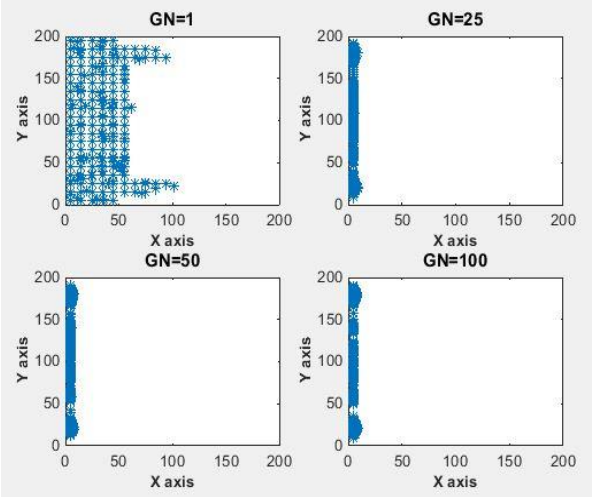

Fig. 16 The optimal locations of the patches in the CFFF condition in 2-dimentional space

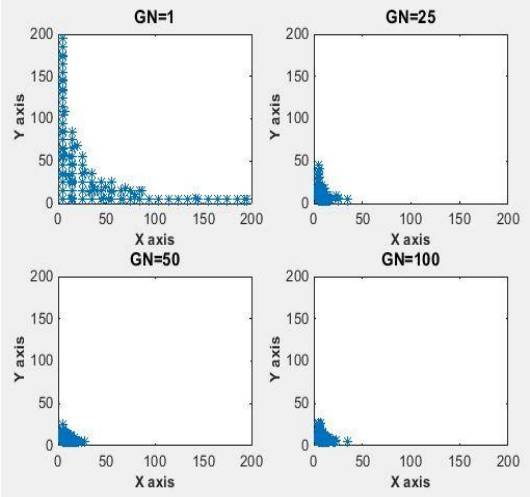

Fig. 19 The optimal locations of the patches in the CCFF condition in 2-dimentional space

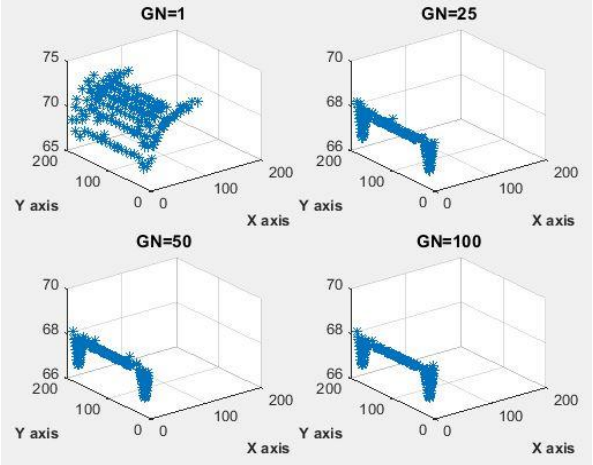

Fig. 17 The optimal locations of the patches in the CFFF condition in 3-dimentional space

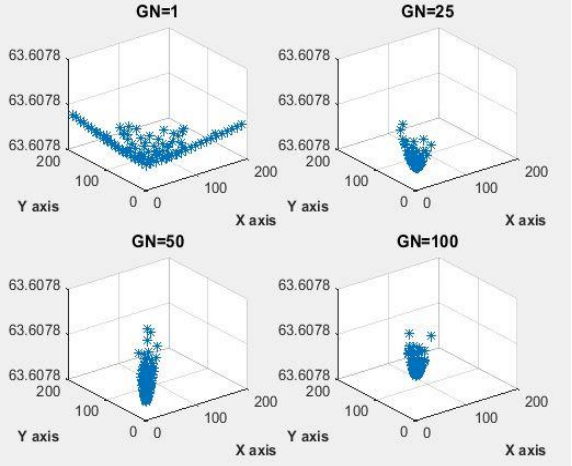

Fig. 20 The optimal locations of the patches in the CCFF condition in 3-dimentional space

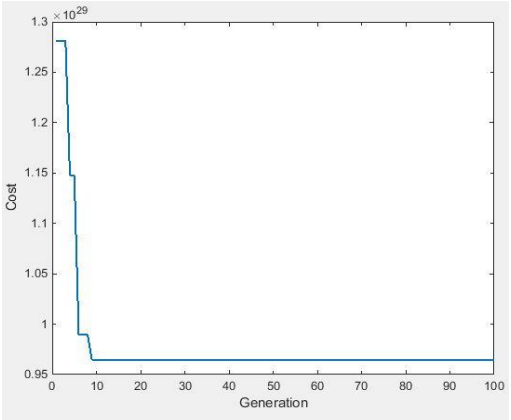

Fig. 18 Variation of fitness value with generation number in the CFFF condition

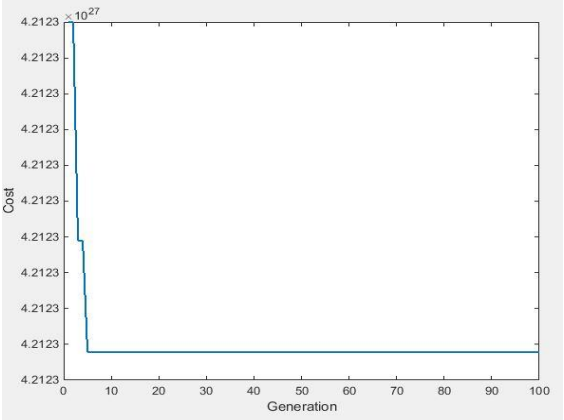

Fig. 21 Variation of fitness value with generation number in the CCFF condition

constraints: SSSS, CFFF and CCFF.

In SSSS conditions, the actuator/sensor patches pair deals with four corners. Therefore, it is obviously the lowest vibration in the sandwich panel. A piezoelectric patch for each corner of the plate can be a proper selection. The results of the optimum position of patches are shown in

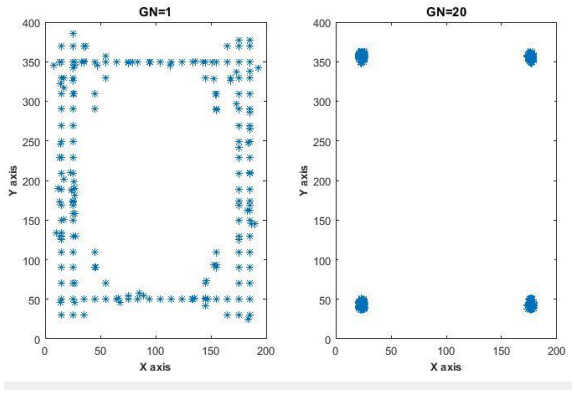

Fig. 22 The optimal locations of the patches in the SSSS condition in 2-dimentional space for a rectangular shape

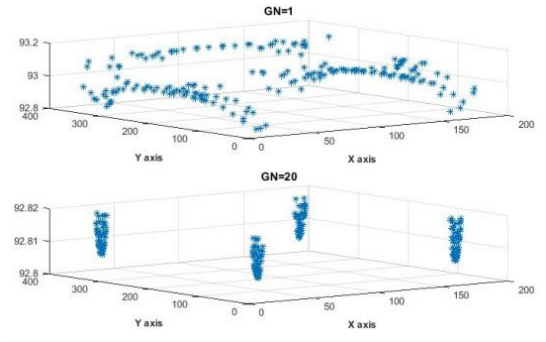

Fig. 23 The optimal locations of the patches in the SSSS condition in 3-dimentional space for a rectangular shape

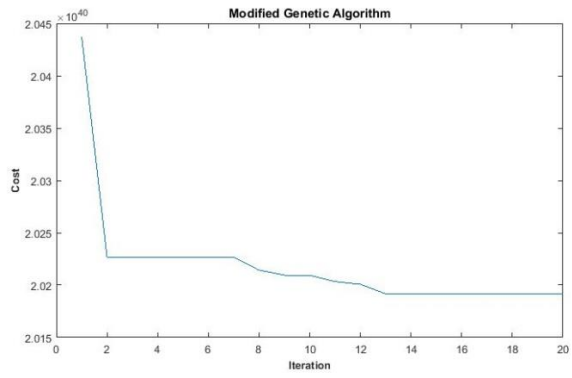

Fig. 24 Variation of fitness values in the SSSS condition for a rectangular shape

Figs. 11 to 14, and presented in 2-dimentional space and 3-dimentional space, respectively. The optimal placement of actuator/sensor pairs is shown in the 2-dimentional space and cost function value is added as the third dimension in logarithm unit in the 3-dimentional space. Some figures for the rectangular and square shapes in different dimensions up to 20 iterations have been considered in Figs. 11-14.

In the present study, the optimum placement of patches is determined by Eq. (21) that have the best convergence. In Fig. 15, the vibration of the sandwich plates damps in lower than 10 generations.

In CFFF conditions, the actuator/sensor patches pair deals with the clamped side (x = 0). The results of the optimum placement of patches are shown in Figs. 16 and 17, in 2-dimentional space and 3-dimentional space, respectively.

As seen in Fig. 18, the quick convergence of the algorithm for a plate with a clamped boundary condition (x = 0) occurs with the omission of the repeated cost functions and proper selection of the primary population. The convergence can also be observed in four steps and in less than 10 generations.

Figs. 19-20 demonstrate the optimal displacement of the piezoelectric actuator/sensor patches pair in a clamped plate in two sides (x = 0, y = 0). The convergence occurred near the origin by less than 25 generations. The third dimension in Fig. 19 is the cost function value, the optimal placement for the piezoelectric patch is the origin, and the distribution of the piezoelectric patches in the plate is almost symmetric and will be symmetric with the increase of the number of the generations.

Fig. 21 shows convergence progress to the optimal solution by plotting the best member at generation and the results indicate that the optimal solution is global and that the convergence occurred in 2 steps and less than 10 generations.

For simply supported boundary condition, a logarithmic value of the cost function for the 3D case is found to be around 92.6, while for CFFF and CCFF cases in Figs. 16 and 20, a logarithmic value of the cost function is around 63.6078. It is noted that the value of 92.6 is a logarithmic value of the cost function and it is not the location of patch.

Fig. 11 shows the more number of iterations is, the more the cost values will converge to the four angles of the plate. In SSSS condition, the cost values converge to the four angles with the minimum vibration and the minimum energy (cost value). Furthermore, in CCFF and CFFF boundary conditions, the cost values converge to the clamped face. The value of 63.6078 is a logarithmic value of the cost function that is equal to $\exp(63.6078) = 4.21 \times 10^{27}$.

Figs. 22-24 show the convergence of the cost values for a rectangular shape in 20 iterations.

7. Conclusions

The present study investigated the optimum placement of patches to suppress the vibration of a sandwich plate. This study examined the stability by running the genetic algorithm program several times. In each run, the optimal fitness was the same via different routes, which is indicative of the correctness and stability. The present study showed the effectiveness of GA on the optimal displacement of actuator/ sensor patches pair in the active vibration control of a sandwich panel. The results were investigated for three boundary conditions including SSSS, CFFF and CCFF. The dynamic equations of a sandwich panel based on classical plate theory are proposed. The optimum position of patches

is determined by LQR and GA. The repeated patches on the chromosome are omitted by filtering methods. The results were investigated for three boundary conditions, SSSS, CFFF and CCFF. However, finding the best position for the actuator/sensor patches pair decreased more control energy and therefore the cost of the control system. Proper selection of the parent and the omission of the repeated chromosome increased the convergence to the best placement for the actuator/sensor patches pair to a large extent.

Acknowledgments

The authors would like to thank the referees for their valuable comments. Also, they are thankful to the University of Kashan for supporting this work by Grant No. 891238/8 and the Iranian Nanotechnology Development Committee for their financial support.

References

Aglietti, G.S., Langley, R.S., Rogers, E. and Gabriel, S.B. (2004), "Model building and verification for active control of microvibrations with probabilistic assessment of the effects of uncertainties", *Proc. Inst. Mech. Eng. C J. Mech. Eng. Sci.*, **218**, 389-399. https://doi.org/10.1177/095440620421800404.

AkhavanAlavi, S.M., Mohammadimehr, M. and Edjtahed, S.H. (2019), "Active control of micro Reddy beam integrated with functionally graded nanocomposite sensor and actuator based on linear quadratic regulator method", *Eur. J. Mech. A Solids*, **74**, 449-461. https://doi.org/10.1016/j.euromechsol.2018.12.008.

Alipour, A. and Zareian, F. (2008), "Study Rayleigh damping in structures; unceratinties and treatments", *Proceedings of the 14th World Conference on Earthquake Engineering*, Beijing, China, October.

Amini, A., Mohammadimehr, M. and Faraji, A. (2019), "Active control to reduce the vibration amplitude of the solar honeycomb sandwich panels with CNTRC facesheets using piezoelectric patch sensor and actuator", *Steel Compos. Struct., Int. J.*, **32**(5), 671-686. https://doi.org/10.12989/scs.2019.32.5.671.

Argha, A., Su, S.W., Savkin, A. and Celler, B. (2019), "A framework for optimal actuator/sensor selection in a control system", *Int. J. Control*, **92**(2), 242-260. https://doi.org/10.1080/00207179.2017.1350755.

Ashwin, U., Raja, S. and Dwarakanathan, D. (2009), "A finite element based substructuring procedure for design analysis of large smart structural system", *Smart Mater. Struct.*, **18**(4), 045006. https://doi.org/10.1088/0964-1726/18/4/045006.

Babaeeian, M. and Mohammadimehr, M. (2020), "Investigation of the time elapsed effect on residual stress measurement in a composite plate by DIC method", *Opt. Lasers Eng.*, **128**, 106002. https://doi.org/10.1016/j.optlaseng.2020.106002.

Bendine, K., Boukhoulda, F.B., Haddag, B. and Nouari, M. (2019), "Active vibration control of composite plate with optimal placement of piezoelectric patches", *Mech. Adv. Mater. Struct.*, **26**(4), 341-349. https://doi.org/10.1080/15376494.2017.1387324.

Daraji, A., Hale, J.M. and Ye, J. (2017), "New methodology for optimal placement of piezoelectric sensor/actuator pairs for active vibration control of flexible structures", *ASME J. Vib. Acoust.*, **140**(1), 011015. https://doi.org/10.1115/1.4037510.

Demetriou, M.A. (2000), "A numerical algorithm for the optimal placement of actuators and sensors for flexible structures", *Proceedings of the 2000 American Control Conference*, Chicago, USA, June.

Demetriou, M.A. and Borggaard, J. (2003), "Optimization of an integrated actuator placement and robust control scheme for distributed parameter processes subject to worst-case spatial disturbance distribution", *Proceedings of the 2003 American Control Conference*, Denver, USA, June.

Dorato, P., Abdallah, C.T. and Cerone, V. (2000), *Linear Quadratic Control: An Introduction*, Krieger Publishing Company, Florida, USA.

Ghasemi A.R. and Meskini, M. (2019), "Free vibration analysis of porous laminated rotating circular cylindrical shells", *J. Vib. Control*, **25**(18), 2494-2508. https://doi.org/10.1177/1077546319858227.

Ghasemi, H., Park, H.S. and Rabczuk, T. (2017), "Level-set based IGA formulation for topology optimization of flexoelectric materials", *Comput. Methods Appl. Mech. Eng.*, **313**, 239-258. https://doi.org/10.1016/j.cma.2016.09.029.

Ghasemi, H., Park, H.S. and Rabczuk, T. (2018), "A multi-material level set-based topology optimization of flexoelectric composites", *Comput. Methods Appl. Mech. Eng.*, **332**, 47-62. https://doi.org/10.1016/j.cma.2017.12.005.

Ghorbanpour Arani, A., Rousta Navi, B. and Mohammadimehr, M. (2016), "Surface stress and agglomeration effects on nonlocal biaxial buckling polymeric nanocomposite plate reinforced by CNT using various approaches", *Adv. Compos. Mater.*, **25**(5), 423-441. https://doi.org/10.1080/09243046.2015.1052189.

Ilchmann, A., Leben, L., Witschel, J. and Worthmann, K. (2018), "Optimal control of differential-algebraic equations from an ordinary differential equation perspective", *Optim. Control Appl. Methods*, **40**(2), 351-366. https://doi.org/10.1002/oca.2481.

Jia, S. and Shan, J. (2018), "Optimal actuator placement for constrained gyroelastic beam considering control spillover", *J. Guid. Control Dyn.*, **41**(9), 2073-2081. https://doi.org/10.2514/1.G003560.

Kumar, K.R. and Narayanan, S. (2007), "The optimal location of piezoelectric actuators and sensors for vibration control of plates", *Smart Mater. Struct.*, **16**(6), 2680. https://doi.org/10.1088/0964-1726/16/6/073.

Manohar, K., Nathan Kutz, J. and Brunton, S. (2018), "Optimal sensor and actuator placement using balanced model reduction", *arXiv*, **2018**, 1812.01574.

Martynowicz, P. (2019), "Real-time implementation of nonlinear optimal-based vibration control for a wind turbine model", *J. Low Freq. Noise Vib. Active Control*, **38**(3-4), 1635-1650. https://doi.org/10.1177/1461348418793346.

Mohammadimehr, M. and Mehrabi, M. (2018), "Electro-thermo-mechanical vibration and stability analyses of double-bonded micro composite sandwich piezoelectric tubes conveying fluid flow", *Appl. Math. Model.*, **60**, 255-272. https://doi.org/10.1016/j.apm.2018.03.008.

Mohammadimehr, M., Mohammadimehr, M.A. and Dashti, P. (2016), "Size-dependent effect on biaxial and shear nonlinear buckling analysis of nonlocal isotropic and orthotropic micro-plate based on surface stress and modified couple stress theories using differential quadrature method", *Appl. Math. Mech.*, **37**(4), 529-554. https://doi.org/10.1007/s10483-016-2045-9.

Mohammadimehr, M., Mohammadi-Dehabadi, A.A. and Maraghi, Z.K. (2017), "The effect of non-local higher order stress to predict the nonlinear vibration behavior of carbon nanotube conveying viscous nanoflow", *Physica B Condens. Matter*, **510**, 48-59. https://doi.org/10.1016/j.physb.2017.01.014.

Mohammadimehr, M., Emdadi, M., Afshari, H. and Rousta Navi, B. (2018a), "Bending, buckling and vibration analyses of MSGT microcomposite circular-annular sandwich plate under hydro-thermo-magneto-mechanical loadings using DQM", *Int. J. Smart Nano Mater.*, **9**(4), 233-260.

https://doi.org/10.1080/19475411.2017.1377312.
Mohammadimehr, M., Mohammadi-Dehabadi, A.A., Alavi, S.M.A., Alambeigi, K., Bamdad, M., Yazdani, R. and Hanifehlou, S. (2018b), "Bending, buckling and free vibration analyses of carbon nanotube reinforced composite beams and experimental tensile test to obtain the mechanical properties of nanocomposite", *Steel Compos. Struct., Int. J.*, **29**(3), 405-422. http://dx.doi.org/10.12989/scs.2018.29.3.405.
Nanthakumar, S.S., Lahmer, T., Zhuang, X., Zi, G. and Rabczuk, T. (2017), "Detection of material interfaces using a regularized level set method in piezoelectric structures", *Inverse Probl. Sci. Eng.*, **24**(1), 153-176. http://dx.doi.org/10.1080/17415977.2015.1017485.
Nestorović, T., Trajkov, M. and Garmabi, S.M. (2015), "Optimal placement of piezoelectric actuators and sensors on a smart beam and a smart plate using multi-objective genetic algorithm", *Smart Struct. Syst., Int. J.*, **15**(4), 1041-1062. https://doi.org/10.12989/sss.2015.15.4.1041.
Ogata, K. (2010), *Modern Control Engineering*, Prentice Hall, India.
Rajabi, J. and Mohammadimehr, M. (2019), "Bending analysis of a micro sandwich skew plate using extended Kantorovich method based on Eshelby-Mori-Tanaka approach", *Comput. Concrete, Int. J.*, **23**(5), 361-376. http://dx.doi.org/10.12989/cac.2019.23.5.361.
Rao, K.V., Raja, S. and Gowda, T.M. (2014a), "Finite element modeling and bending analysis of piezoelectric sandwich beam with debonded actuators", *Smart Struct. Syst., Int. J.*, **13**(1), 55-80. https://doi.org/10.12989/sss.2014.13.1.055.
Rao, K.V., Raja, S. and Munikenche, T. (2014b), "Finite element modeling and bending analysis of piezoelectric sandwich beam with debonded actuators", *Smart Struct. Syst., Int. J.*, **13**(1), 55-80. https://doi.org/10.12989/sss.2014.13.1.055.
Rostami, R., Irani, M. and Mohammadimehr, M. (2019), "Vibration control of the rotating sandwich cylindrical shell considering functionally graded core and functionally graded magneto-electro-elastic layers by using differential quadrature method", *J. Sandw. Struct. Mater.*, **2019**, 1099636218824139. https://doi.org/10.1177/1099636218824139.
Rudolf, C., Martin, T. and Wauer, J. (2010), "Control of PKM machine tools using piezoelectric self-sensing actuators on basis of the functional principle of a scale with a vibrating string", *Smart Struct. Syst., Int. J.*, **6**(2), 167-182. https://doi.org/10.12989/sss.2010.6.2.167.
Sakha, M.S., Shaker, H.R. and Tahavori, M. (2017), "Optimal sensors and actuators placement for large-scale switched systems", *Int. J. Dyn. Control*, **7**(1), 147-156. https://doi.org/10.1007/s40435-018-0446-7.
Tanimoto, Y., Nishiwaki, T., Shiomi, T. and Maekawa, Z. (2001), "A numerical modeling for eigenvibration analysis of honeycomb sandwich panels", *Compos. Interf.*, **8**(6), 393-402. https://doi.org/10.1163/156855401753424433.
Tham, V.V, Quoc, T.H. and Tu, T.M. (2018), "Optimal placement and active vibration control of composite plates integrated piezoelectric sensor/actuator pairs", *Viet. J. Sci. Technol.*, **56**. 113. https://doi.org/10.15625/2525-2518/56/1/8824.
Xue, K., Igarashi, A. and Kachi, T. (2018), "Optimal sensor placement for active control of floor vibration considering spillover effect associated with modal filtering", *Eng. Struct.*, **165**, 198-209. https://doi.org/10.1016/j.engstruct.2018.03.024.
Yang, B., Miao, J., Fan, Z., Long, J. and Liu, X. (2018), "Modified cuckoo search algorithm for the optimal placement of actuators problem", *Appl. Soft Comput.*, **67**, 48-60. https://doi.org/10.1016/j.asoc.2018.03.004.
Yassin, B., Lahcen, A. and Zeriab, E.S.M. (2018), "Hybrid optimization procedure applied to optimal location finding for piezoelectric actuators and sensors for active vibration control", *Appl. Math. Model.*, **62**, 701-716. https://doi.org/10.1016/j.apm.2018.06.017.
Yin, H., Dong, K., Pan, A., Peng, Z., Jiang, Z. and Li, S. (2019), "Optimal sensor placement based on relaxation sequential algorithm", *Neurocomputing*, **344**, 28-36. https://doi.org/10.1016/j.neucom.2018.03.088.
Zare, A., Mohammadi, H., Dhingra, N.K., Jovanović, M.R. and Georgiou, T.T. (2018), "Proximal algorithms for large-scale statistical modeling and optimal sensor/actuator selection", *arXiv*, **2018**, 1807.01739.

CC

Appendix A

Normal and shear strain relations can be obtained as follows

$$\begin{Bmatrix}\varepsilon_{xx}\\ \varepsilon_{yy}\\ \gamma_{xy}\end{Bmatrix}=\begin{Bmatrix}\frac{\partial U}{\partial x}\\ \frac{\partial V}{\partial y}\\ \frac{\partial U}{\partial y}+\frac{\partial V}{\partial x}\end{Bmatrix}=\begin{Bmatrix}\frac{\partial u}{\partial x}\\ \frac{\partial v}{\partial y}\\ \frac{\partial u}{\partial y}+\frac{\partial v}{\partial x}\end{Bmatrix}+z\begin{Bmatrix}-\frac{\partial^2 w}{\partial x^2}\\ -\frac{\partial^2 w}{\partial y^2}\\ -2\frac{\partial^2 w}{\partial x\partial y}\end{Bmatrix} \quad \text{(A1)}$$

$$\begin{Bmatrix}\gamma_{xz}\\ \gamma_{yz}\end{Bmatrix}=\begin{Bmatrix}0\\ 0\end{Bmatrix}$$

The constitutive equations for the sandwich plate composed of homogenous aluminum honeycomb core and nanocomposite facesheets are written as follows

$$\begin{Bmatrix}\sigma_{xx}\\ \sigma_{yy}\\ \sigma_{xy}\\ \sigma_{yz}\\ \sigma_{xz}\end{Bmatrix}=\begin{bmatrix}Q_{11} & Q_{12} & 0 & 0 & 0\\ Q_{12} & Q_{22} & 0 & 0 & 0\\ 0 & 0 & Q_{66} & 0 & 0\\ 0 & 0 & 0 & Q_{44} & 0\\ 0 & 0 & 0 & 0 & Q_{55}\end{bmatrix}\begin{Bmatrix}\varepsilon_{xx}\\ \varepsilon_{yy}\\ \gamma_{xy}\\ \gamma_{yz}\\ \gamma_{xz}\end{Bmatrix} \quad \text{(A2)}$$

$$\varepsilon_{zz}=0 \quad \text{(A3)}$$

$$Q_{11}=\frac{E_{11}}{1-\nu_{12}\nu_{21}},\qquad Q_{12}=\frac{\nu_{21}E_{11}}{1-\nu_{12}\nu_{21}}$$
$$Q_{22}=\frac{E_{22}}{1-\nu_{12}\nu_{21}},\qquad Q_{66}=G_{12}=\frac{E_{11}}{2(1+\nu_{21})} \quad \text{(A4)}$$
$$Q_{44}=G_{23},\qquad Q_{55}=G_{13}$$

In Eq. (A4), E_{11}, E_{22}, ν_{12}, G_{13}, G_{23}, G_{12} and Q parameters are Yang moduli in x and y directions, Poisson's ratio, shear moduli in three directions and stress constants, respectively.

Appendix B

Kinetic energy

To compute the kinetic energy of the solar panel, the energy of each layer including the core, composite reinforced by carbon nanotube facesheets, piezoelectric layers, and the lumped mass must be calculated in the following form

$$T= T_c + T_{fs_t} + T_{fs_b} + T_{pzs_t} + T_{pzs_b} + T_{pza_t} + T_{pza_b} + T_{lm} \quad \text{(B1)}$$

The general equation to calculate kinetic energy is

$$\mathrm{T} = \int \frac{1}{2}\rho\left(\left(\frac{\partial U}{\partial t}\right)^2 + \left(\frac{\partial V}{\partial t}\right)^2 + \left(\frac{\partial W}{\partial t}\right)^2\right)\mathrm{dV} = \frac{1}{2}\dot{\Gamma}^T M \dot{\Gamma} \quad \text{(B2)}$$

where p denotes the material density.

Potential energy:

The total potential energy of the sandwich plate is derived from the sum of core, CNTRC facesheets, piezoelectric layers and the lumped mass potential energies.

$$U= U_c + U_{fst} + U_{fsb} + U_{pzs_t} + U_{pzs_b} + U_{pza_t} + U_{pza_b} \quad \text{(B3)}$$

For the homogenous core of the sandwich panel, the potential energy is written as follows

$$U_c = \frac{1}{2}\int_0^{\mathrm{a}}\int_0^{\mathrm{b}}\int_{\frac{-\mathrm{h_c}}{2}}^{\frac{\mathrm{h_c}}{2}} \varepsilon^T \sigma_c \,\mathrm{dxdydz} = \frac{1}{2}\Gamma^T K_c \Gamma \quad \text{(B4)}$$

where

$$K_c = \int_0^{\mathrm{a}}\int_0^{\mathrm{b}}\int_{\frac{-\mathrm{h_c}}{2}}^{\frac{\mathrm{h_c}}{2}} \begin{pmatrix} (Q_{11\mathrm{c}}\left(z^2 \frac{\partial^2 \mathrm{N}}{\partial \mathrm{x}^2}\frac{\partial^2 \mathrm{N}^{\mathrm{T}}}{\partial \mathrm{x}^2}\right) \\ + Q_{22\mathrm{c}}\left(z^2 \frac{\partial^2 \mathrm{N}}{\partial \mathrm{y}^2}\frac{\partial^2 \mathrm{N}^{\mathrm{T}}}{\partial \mathrm{y}^2}\right) \\ + 2Q_{12\mathrm{c}}\left(z^2 \frac{\partial^2 \mathrm{N}}{\partial \mathrm{x}^2}\frac{\partial^2 \mathrm{N}^{\mathrm{T}}}{\partial \mathrm{y}^2}\right) \\ + Q_{66\mathrm{c}}\left(4z^2 \frac{\partial^2 \mathrm{N}}{\partial \mathrm{x}\partial \mathrm{y}}\frac{\partial^2 \mathrm{N}^{\mathrm{T}}}{\partial \mathrm{x}\partial \mathrm{y}}\right)) \end{pmatrix} \mathrm{dxdydz} \quad \text{(B5)}$$

And for the CNTRC facesheet, the potential energy is obtained from the following expression

$$U_{fs} = \frac{1}{2}\iiint \varepsilon^T \sigma_{fs} \mathrm{dxdydz} = \frac{1}{2}\Gamma^T K_{fs} \Gamma \quad \text{(B6)}$$

where

$$K_{fs} = \iiint \begin{pmatrix} (Q_{11\mathrm{f}}\left(z^2 \frac{\partial^2 \mathrm{N}}{\partial \mathrm{x}^2}\frac{\partial^2 \mathrm{N}^{\mathrm{T}}}{\partial \mathrm{x}^2}\right) + \\ Q_{22\mathrm{f}}\left(z^2 \frac{\partial^2 \mathrm{N}}{\partial \mathrm{y}^2}\frac{\partial^2 \mathrm{N}^{\mathrm{T}}}{\partial \mathrm{y}^2}\right) \\ + 2Q_{12\mathrm{f}}\left(z^2 \frac{\partial^2 \mathrm{N}}{\partial \mathrm{x}^2}\frac{\partial^2 \mathrm{N}^{\mathrm{T}}}{\partial \mathrm{y}^2}\right) \\ + Q_{66\mathrm{f}}\left(4z^2 \frac{\partial^2 \mathrm{N}}{\partial \mathrm{x}\partial \mathrm{y}}\frac{\partial^2 \mathrm{N}^{\mathrm{T}}}{\partial \mathrm{x}\partial \mathrm{y}}\right)) \end{pmatrix} \mathrm{dxdydz} \quad \text{(B7)}$$

the potential energy for the piezoelectric patch.

$$U_{pz_{elast}} = \sum_{\mathrm{i}=1}^{N_{pz}} \frac{1}{2}\iiint \varepsilon^T \sigma_{pzi} \mathrm{dxdydz} = \frac{1}{2}\Gamma^T K_{pz_{elast}} \Gamma \quad \text{(B8)}$$

$$K_{pz_{elast}} = \sum_{\mathrm{i}=1}^{\mathrm{N_{pz}}} \iiint \begin{pmatrix} \frac{E_{pzi}\mathrm{z}^2}{(1-\upsilon_{pzi}^2)}[\frac{\partial^2 N_{pzi}}{\partial \mathrm{x}^2}\frac{\partial^2 N_{pzi}}{\partial \mathrm{x}^2}^{\mathrm{T}} \\ + \frac{\partial^2 N_{pzi}}{\partial \mathrm{y}^2}\frac{\partial^2 N_{pzi}}{\partial \mathrm{y}^2}^{\mathrm{T}} \\ + 2\upsilon_{pzi}\frac{\partial^2 N_{pzi}}{\partial \mathrm{x}^2}\frac{\partial^2 N_{pzi}}{\partial \mathrm{y}^2}^{\mathrm{T}} \\ + 2(1-\upsilon_{pzi})\frac{\partial^2 N_{pzi}}{\partial \mathrm{x}\partial \mathrm{y}}\frac{\partial^2 N_{pzi}}{\partial \mathrm{x}\partial \mathrm{y}}^{\mathrm{T}}]\mathrm{dxdydz} \end{pmatrix} \quad \text{(B9)}$$

The elastoelectric energy stored in the N_{pz} patches can be written as

$$U_{pz_{elastelect}} = V_{pz}{}^T K_{pz_{elastelect}} \Gamma \quad \text{(B10)}$$

$$K_{pz_{elastelect}} = \sum_{\mathrm{i}=1}^{\mathrm{N_{pz}}} \iiint \frac{E_{pz_i}\epsilon_{z_i} p_i}{2(1-\upsilon_{pz_i})}\begin{pmatrix} z\frac{\partial^2 N_{pzi}}{\partial \mathrm{x}^2}^{\mathrm{T}} \\ + \mathrm{z}\frac{\partial^2 N_{pzi}}{\partial \mathrm{y}^2}^{\mathrm{T}} \end{pmatrix} \mathrm{dxdydz} \quad \text{(B11)}$$

$$U_{pz_{elect}} = \frac{1}{2} V^T K_{pz_{elect}} V \quad \text{(B12)}$$

$$K_{pz_{elect}} = \sum_{\mathrm{i}=1}^{\mathrm{N_{pz}}} \iiint \epsilon_{pz_i} P_i{}^T P_i \mathrm{dxdydz} \quad \text{(B13)}$$

Therefore, the general relation for the potential energy is

$$\begin{aligned} U= \frac{1}{2}\Gamma^T K_c \Gamma + \frac{1}{2}\Gamma^T K_{fs} \Gamma + \frac{1}{2}\Gamma^T K_{pz_{elast}} \Gamma \\ + V_{pz}{}^T K_{pz_{elastelect}} \Gamma + \frac{1}{2} V_{pz}{}^T K_{pz_{elect}} V_{pz} \end{aligned} \quad \text{(B14)}$$

By employing the kinetic and potential energies and the generalized forces and derivation of Γ and V_{pz} yields the following equations

$$\begin{aligned} &\left(M_c + M_{fs} + M_{pz}\right)\ddot{\Gamma} + C_s\dot{\Gamma} \\ &+ \left(K_c + K_{fs} + K_{pz_{elast}}\right)\Gamma + K_{pz_{elastelect}}^T V_{pz} = N_f^T F \end{aligned} \quad \text{(B15)}$$

$$K_{pz_{elastelect}} \Gamma + K_{pz_{elastelect}}^T V_{pz} = 0 \quad \text{(B16)}$$

By defining the following term, we have

$$M= M_c + M_{fs} + M_{pz} \quad \text{(B17)}$$

$$K_{elast} = K_c + K_{fs} + K_{pz_{elast}} \quad \text{(B18)}$$

By substituting Eqs. (B12) and (B13) into Eqs. (B10), the governing equation can be written as follows

$$\begin{cases} M\ddot{\Gamma} + C_s\dot{\Gamma} + K_{elast}\Gamma + K_{pza_{elastelect}}^T V_{pza} = N_f^T F \\ K_{pz_{elastelect}} \Gamma + K_{pz_{elastelect}}^T V_{pz} = 0 \end{cases} \quad \text{(B19)}$$

where

$$K^T_{pz_{elastelect}} V_{pz} = \begin{bmatrix} K^T_{pzs_{elastelect}} & K^T_{pza_{elastelect}} \end{bmatrix} \begin{bmatrix} V_{pzs} \\ V_{pza} \end{bmatrix} \quad \text{(B20)}$$

Inputs to GA are the locations of sensors and actuators that are determined by x and y coordinates in Eqs.(3)-(5). Parameter ($N_{m,n}(x,y)$) is directly related to the placement. In the final equation (Eq. (B14)), M, K, $K_{pz_{elastelect}}$ and N_f parameters are related to x and y positions that we have

$$\begin{aligned} \mathrm{M} &= \iiint \rho \left(z^2 \frac{\partial \mathrm{N}}{\partial \mathrm{x}} \frac{\partial \mathrm{N}^{\mathrm{T}}}{\partial \mathrm{x}} + \mathrm{z}^2 \frac{\partial \mathrm{N}}{\partial \mathrm{y}} \frac{\partial \mathrm{N}^{\mathrm{T}}}{\partial \mathrm{y}} + \mathrm{N}.\mathrm{N}^{\mathrm{T}} \right) \mathrm{dxdydz} \\ \mathrm{K} &= \iiint \begin{pmatrix} (Q_{11\mathrm{c}} \left(z^2 \frac{\partial^2 \mathrm{N}}{\partial \mathrm{x}^2} \frac{\partial^2 \mathrm{N}^{\mathrm{T}}}{\partial \mathrm{x}^2} \right) \\ + Q_{22\mathrm{c}} \left(z^2 \frac{\partial^2 \mathrm{N}}{\partial \mathrm{y}^2} \frac{\partial^2 \mathrm{N}^{\mathrm{T}}}{\partial \mathrm{y}^2} \right) \\ + 2 Q_{12\mathrm{c}} \left(z^2 \frac{\partial^2 \mathrm{N}}{\partial \mathrm{x}^2} \frac{\partial^2 \mathrm{N}^{\mathrm{T}}}{\partial \mathrm{y}^2} \right) \\ + Q_{66\mathrm{c}} \left(4 z^2 \frac{\partial^2 \mathrm{N}}{\partial \mathrm{x} \partial \mathrm{y}} \frac{\partial^2 \mathrm{N}^{\mathrm{T}}}{\partial \mathrm{x} \partial \mathrm{y}} \right)) \end{pmatrix} \mathrm{dxdydz} \\ K_{pz_{elastelect}} &= \sum_{\mathrm{i}=1}^{\mathrm{N_{pz}}} \iiint \frac{E_{pz_i} \epsilon_{z_i} p_i}{2(1 - \upsilon_{pz_i})} \begin{pmatrix} \mathrm{z} \frac{\partial^2 N_{\mathrm{pzi}}{}^T}{\partial x_{pz}{}^2} \\ + \mathrm{z} \frac{\partial^2 N_{pzi}{}^T}{\partial y_{pz}{}^2} \end{pmatrix} \mathrm{dxdydz} \\ N_f(x, y) &= \sin\left(\frac{m\pi x_f}{a}\right) \sin\left(\frac{n\pi y_f}{b}\right) \end{aligned} \quad \text{(B21)}$$

It is noted that the limits of integration of variables (M_{pz}, K_{pz}, $\mathrm{K_{pz_{elastelect}}}$, N_f) depend on the position of piezoelectric patch pairs. For example, the following equations have been obtained in the position of a piezo patch ($110 < x_{pz} < 130,\ 50 < y_{pz} < 60,\ 10.5 < z_{pz} < 10.69$)

$$\begin{aligned} N_{pz}(x, y) &= \sin\left(\frac{m\pi x_{pz}}{a}\right) \sin\left(\frac{n\pi y_{pz}}{b}\right) \\ M_{pz} &= \int_{110}^{130} \int_{50}^{60} \int_{10.5}^{10.69} \rho_{pz} \begin{pmatrix} z^2 \frac{\partial N_{pz}}{\partial x_{pz}} \frac{\partial N_{pz}{}^T}{\partial x_{pz}} \\ + z^2 \frac{\partial \mathrm{N_{pz}}}{\partial y_{pz}} \frac{\partial N_{pz}{}^T}{\partial y_{pz}} \\ + N_{pz}.N_{pz}{}^T \end{pmatrix} dx_{pz} dy_{pz} dz_{pz} \end{aligned} \quad \text{(B22)}$$